

Dynamic Principal Subspaces with Sparsity in High Dimensions

Xiaoyu Hu and Fang Yao

School of Mathematical Sciences, Center for Statistical Science, Peking University, China

Abstract

Principal component analysis (PCA) is a versatile tool to reduce the dimensionality which has wide applications in statistics and machine learning community. It is particularly useful to model data in high-dimensional scenarios where the number of variables p is comparable to, or much larger than the sample size n . Despite extensive literature on this topic, researches have focused on modeling static principal eigenvectors or subspaces, which is unsuitable for stochastic processes that are dynamic in nature. To characterize the change in the whole course of high-dimensional data collection, we propose a unified framework to estimate dynamic principal subspaces spanned by leading eigenvectors of covariance matrices. In the proposed framework, we formulate an optimization problem by combining the kernel smoothing and regularization penalty together with the orthogonality constraint, which can be effectively solved by the proximal gradient method for manifold optimization. We show that our method is suitable for high-dimensional data observed under both common and irregular designs. In addition, theoretical properties of the estimators are investigated under l_q ($0 \leq q \leq 1$) sparsity. Extensive experiments demonstrate the effectiveness of the proposed method in both simulated and real data examples.

KEYWORDS: Dimension reduction; Local smoothing; Manifold optimization; Principal components; Sparsity.

1. INTRODUCTION

In statistics and machine learning community, PCA is widely used to reduce dimensionality and extract useful features by transforming the original variables into a few of new variables while retaining most information in the data. With significant advances of science and technology, high-dimensional data, where the number of variables p is comparable to, or much larger than the sample size n , becomes pervasive. To effectively model high-dimensional data and enhance its interpretability, sparse PCA methodologies have been developed with various structural assumptions (e.g., [Johnstone and Lu, 2009](#); [Ma, 2013](#); [Vu et al., 2013](#)). Existing works in this field mainly focus on estimating static principal eigenvectors or subspaces. However, the principal subspaces often

possess dynamic structures, especially for random processes, which makes these previous methods less desirable. To tackle this issue, we aim to dynamically estimate the principal subspaces spanned by leading eigenvectors of covariance matrices throughout the entire course of data collection, which is referred to as the dynamic PCA.

There are extensive literature estimating the principal eigenvectors or subspaces which are treated as static for high-dimensional data. For spiked covariance models, [Johnstone and Lu \(2009\)](#) proposed diagonal thresholding algorithm to obtain the first leading eigenvector by retaining variables with large sample variances, and [Ma \(2013\)](#) refined such estimation by an iterative thresholding approach. In more general settings, [Vu and Lei \(2013\)](#) introduced two complementary notions of subspace sparsity and gave the non-asymptotic lower and upper bound on the minimax subspace estimation error. For the optimization-based methods, [Zou et al. \(2006\)](#) formulated it as a elastic net regression-type problem to obtain sparse loadings. [Shen and Huang \(2008\)](#) proposed a low rank matrix approximation approach. [Witten et al. \(2009\)](#) presented a penalized matrix decomposition, while [Vu et al. \(2013\)](#) proposed a convex relaxation based on the convex hull of low rank projection matrices. However, these aforementioned methods and theories are not applicable for modeling potentially varying structures in the principal subspaces, which motivates us to study a dynamic model.

Closely related to this paper, some works have made early explorations of dynamic covariance models. For instance, [Yin et al. \(2010\)](#) constructed a Nadaraya-Waston estimator, which however only works well in low-dimensional settings. Moreover, by treating the covariance matrices as responses that lie in Riemannian manifold, a semiparametric estimator ([Zhu et al., 2009](#)) and a local polynomial estimator ([Yuan et al., 2012](#)) are developed, respectively. For high-dimensional data, [Chen and Leng \(2016\)](#) proposed a dynamic covariance model making use of kernel smoothing and thresholding. However, these existing works did not account for the dependence among observations from the same individual which is an important nature of repeated measurements ([Cai and Yuan, 2011](#)). Our numerical studies reveal that the principal subspaces deduced by dynamic covariance estimation ([Chen and Leng, 2016](#)) cannot perform well, especially when the observational grids are sparse and the dimension is high, see [Sections 4 and 5](#). Another related work is [Berrendero et al. \(2011\)](#) who proposed to estimate the principal eigenvectors using the sample covariance matrices

which is infeasible for irregularly spaced data and high-dimensional settings.

In this work, we propose a unified framework and formulate an optimization problem on Stiefel manifold to estimate the dynamic principal subspaces for high-dimensional data, which combines the kernel smoothing and sparse regularization. The proposed method has some remarkable features. First, it can be applied to handle functional data under both common and irregular designs (Cai and Yuan, 2011). Second, the formulated optimization problem leads to estimation satisfying sparsity and orthogonality simultaneously, which can be effectively solved by the proximal gradient method for manifold optimization (Chen et al., 2020). Third, our procedure consists of two steps, the first step to obtain an initial estimate from the optimization, and the refining step to improve the estimates by hard thresholding and then re-optimizing on the reduced set of variables. The two-step algorithm helps successfully identify significant features and enhance the interpretability, and entails improved estimates which will be illustrated in numerical studies. The estimators are shown to be consistent under the l_q ($0 \leq q \leq 1$) sparsity. Moreover, we show that the convergence exhibits phase transition phenomenon that attains either nonparametric or parametric rate, depending on the sampling frequency, i.e., how sparse/dense the repeated measurements are observed, see Section 3. It is noteworthy that the convergence rate of principal subspaces is faster than that in dynamic covariance estimation, which coincides with findings in the static case (Vu and Lei, 2012; Bickel and Levina, 2008; Cai and Zhou, 2012).

The remainder of the article is organized as follows. In Section 2.1, we introduce the dynamic PCA, in Section 2.2, we provide the l_q ($0 \leq q \leq 1$) sparsity assumption in dynamic settings and the formulation of our optimization problem, and describe procedures for practical implementation. In Section 3, we present theoretical results for the proposed method under regularity conditions. Simulation results are included in Section 4, followed by an application to the HCP data in Section 5. The details of algorithm and technical proofs are deferred to the Appendix.

2. DYNAMIC PRINCIPAL SUBSPACE WITH SPARSITY

2.1 Dynamic principal subspace

Let $\{\mathbf{X}(t) : t \in \mathcal{T}\}$ be a vector-valued stochastic process defined on a compact interval $\mathcal{T} = [0, 1]$, where $\mathbf{X}(t) = (X_1(t), \dots, X_p(t))^T$. The continuous mean and covariance matrix functions are $\boldsymbol{\mu}(t) = E\mathbf{X}(t)$ and $\boldsymbol{\Sigma}(t) = E\mathbf{X}(t)\mathbf{X}(t)^T - \boldsymbol{\mu}(t)\boldsymbol{\mu}(t)^T$, respectively. For each fixed t , applying

standard PCA, we obtain

$$\mathbf{X}(t) = \boldsymbol{\mu}(t) + \sum_{k=1}^p \xi_k(t) \mathbf{u}_k(t), \quad (1)$$

where $\xi_k(t) = (\mathbf{X}(t) - \boldsymbol{\mu}(t))^T \mathbf{u}_k(t)$ is the k -th principal score with mean zero and variance $\lambda_k(t)$, $\mathbf{u}_k(t)$ is the k -th corresponding eigenvector. Moreover, we have $\text{cov}(\xi_k(t), \xi_l(t)) = 0$ and $\mathbf{u}_k(t)^T \mathbf{u}_l(t) = 0$ for $k \neq l$ at each t . The time-varying version of PCA (1) is called dynamic PCA (DPCA).

Remark 1. *The framework DPCA is essentially different from FPCA (Ramsay and Silverman, 2005; Li and Hsing, 2010), though they both perform principal component analysis on the stochastic process. First, conceptually they view the data from different perspectives. The former treats $\mathbf{X}(t)$ as a vector at each t , while the latter views the random process as an atomic object. Second, technically they represent data in different spaces. The DPCA represents data in the Euclidean space, i.e., it applies standard PCA at each t to obtain $\mathbf{X}(t) = \boldsymbol{\mu}(t) + \sum_{k=1}^p \xi_k(t) \mathbf{u}_k(t)$, where $\mathbf{u}_k(t), k = 1, \dots, p$ form an orthonormal basis in \mathbb{R}^p . By comparison, the FPCA provides a tool to represent $\mathbf{X}(t)$ in the infinite-dimensional function space, i.e., $\mathbf{X}(t) = \sum_{k=1}^{\infty} \theta_k \phi_k(t)$ where θ_k are uncorrelated functional principal scores and $\phi_k(t)$ are orthonormal basis functions in the space of square integrable functions $L^2(\mathcal{T})$. Moreover, instead of the auto-covariance function $C(s, t) = E\mathbf{X}(s)\mathbf{X}(t)^T - \boldsymbol{\mu}(s)\boldsymbol{\mu}(t)^T$, the DPCA requires the much simpler diagonal covariance function $\Sigma(t) = C(t, t)$.*

One advantage of DPCA is the ability to capture the dynamic information contained in data, which facilitates the interpretation. Formally, the principal subspaces of interest are defined to be the solution of the following optimization problem,

$$\begin{aligned} \min_{U(t)} \quad & \int_{\mathcal{T}} E\|\mathbf{X}(t) - \boldsymbol{\mu}(t) - U(t)U(t)^T\{\mathbf{X}(t) - \boldsymbol{\mu}(t)\}\|^2 dt \\ \text{s.t.} \quad & U(t)^T U(t) = I_d, \end{aligned} \quad (2)$$

where $U(t) = (\mathbf{u}_1(t), \dots, \mathbf{u}_d(t)) \in \mathbb{R}^{p \times d}$ and $\mathbf{u}_k(t) = (u_{k1}(t), \dots, u_{kp}(t))^T \in \mathbb{R}^p, k = 1, \dots, d$. The problem (2) is eventually reduced to perform the multivariate PCA pointwise. Therefore, the solution $\mathbf{u}_k(t)$ is the k -th leading eigenvector of $\Sigma(t)$. We refer to the subspaces $\mathcal{S}(t)$ spanned by $U(t)$ as the dynamic principal subspaces of $\Sigma(t)$, and the corresponding projection matrix is given by $\Pi(t) = U(t)U(t)^T$. Denote the eigenvalues by $\lambda_k(t) = \mathbf{u}_k(t)^T \Sigma(t) \mathbf{u}_k(t)$, without loss of

generality, $\lambda_1(t) \geq \lambda_2(t) \geq \dots \geq \lambda_p(t) \geq 0$. We assume that the eigengap $\lambda_d(t) - \lambda_{d+1}(t) > 0$ for all $t \in \mathcal{T}$ so that the d -dimensional principal subspace is well-defined.

Remark 2. *The eigen gap assumption is quite standard in PCA problems. Naturally we assume that it holds over \mathcal{T} in dynamic settings. If the condition $\lambda_d(t) - \lambda_{d+1}(t) > 0, t \in \mathcal{T}$ indeed holds and the covariance matrix function is smooth, then the eigenvector function $\mathbf{u}_d(t)$ (after adjusting the sign) is smooth (Berrendero et al., 2011). One issue that we may encounter is that the eigenvalue functions may intersect, e.g., $\lambda_d(t) = \lambda_{d+1}(t)$ at some t , in this case the corresponding eigenvector function is allowed to be discontinuous at such t . Moreover, it has no much influence on our estimation since we use an estimate $\hat{\Sigma}(t)$ in practice that has eigenvalues of multiplicity 1 with probability 1.*

In reality, we typically have some noisy measurements observed at regular or irregular design points, the observed values are $y_{ijl} = x_{ij}(t_{il}) + \epsilon_{ijl}, t_{il} \in \mathcal{T}$, where ϵ_{ijl} are independent and identically distributed measurement errors independent of x_{ij} with mean zero and variance σ^2 , $i = 1, \dots, n, j = 1, \dots, p$ and $l = 1, \dots, m_i$. We denote $N = \sum_{i=1}^n m_i$ and $\bar{m} = \sum_{i=1}^n m_i/n$. Under the common design, all the observations are sampled at the same locations, i.e., $t_{1l} = t_{2l} = \dots = t_{nl} = t_l$ for all $l = 1, \dots, m$ where $m = \bar{m} = m_1 = \dots = m_n$, while the sampling locations t_{il} are sampled independently from a compact interval \mathcal{T} under the irregular design (Cai and Yuan, 2011).

An empirical version of (2) is formulated by substituting the expectation with its estimate. A naive estimate is to use the sample covariance matrix, which however has some drawbacks. First, since the data are collected at discrete grids, we can merely obtain estimates at observed times instead of the whole course \mathcal{T} . Second, the sample covariance matrices are infeasible under irregular design. Third, the estimates may fluctuate significantly without smoothness regularization. Therefore, a reliable and smooth estimate is more suitable. To illustrate our main idea, we assume $\mu(t) = 0$ for the moment. According to Weyl's inequality, the continuity of $\Sigma(t)$ implies that the $\lambda_k(t)$ is continuous, which ensures that the explained variances by projecting the data at t_{il} onto the neighboring principal subspace at t vary in a continuous manner. Thus, motivated by the kernel smoothing, we propose an empirical optimization problem as follows,

$$\min_{U(t)} \quad \frac{1}{N} \sum_{i=1}^n \sum_{l=1}^{m_i} w_{il}(t) \|\mathbf{y}_{il} - U(t)U(t)^T \mathbf{y}_{il}\|^2 \quad (3)$$

$$s.t. \quad U(t)^T U(t) = I_d,$$

where $w_{il}(t) = K_h(t_{il} - t) / \sum_{i=1}^n \sum_{l=1}^{m_i} K_h(t_{il} - t)$, h is the bandwidth, $K_h(t_{il} - t) = K(|t_{il} - t|/h)/h$ and K is a kernel function. It can be equivalently formulated as

$$\begin{aligned} \max_{U(t)} \quad & \text{Tr}[U(t)^T S_h(t) U(t)] \\ \text{s.t.} \quad & U(t)^T U(t) = I_d, \end{aligned} \tag{4}$$

where $S_h(t) = \sum_{i=1}^n \sum_{l=1}^{m_i} K_h(t_{il} - t) \mathbf{y}_{il} \mathbf{y}_{il}^T / \sum_{i=1}^n \sum_{l=1}^{m_i} K_h(t_{il} - t)$.

Remark 3. *Briefly, a local constant estimator $S_h(t)$ is deduced by the optimization problem (3). Such an estimator has been constantly used in literatures for dynamic covariance model (Yin et al., 2010; Chen and Leng, 2016) with the merit of guaranteeing positive semidefiniteness of covariance matrix, while other estimators, e.g., the local linear estimator or spline-type estimator, may not preserve this property. Thus, we advocate the use of the estimator $S_h(t)$ obtained by (4).*

Note that our proposal can adapt to both common and irregular designs using pooled data. More generally, incorporating the estimated mean function by the kernel smoothing, the estimator $\hat{U}(t)$ can be obtained by substituting $S_h(t)$ in (4) with

$$S_h(t) = \frac{\sum_{i=1}^n \sum_{l=1}^{m_i} K_h(t_{il} - t) \mathbf{y}_{il} \mathbf{y}_{il}^T}{\sum_{i=1}^n \sum_{l=1}^{m_i} K_h(t_{il} - t)} - \frac{\sum_{i=1}^n \sum_{l=1}^{m_i} K_h(t_{il} - t) \mathbf{y}_{il} \sum_{i=1}^n \sum_{l=1}^{m_i} K_h(t_{il} - t) \mathbf{y}_{il}^T}{\{\sum_{i=1}^n \sum_{l=1}^{m_i} K_h(t_{il} - t)\}^2}.$$

Under the common design, the data are observed at regular grids. With theoretical guarantees, practitioners can adopt an alternative estimate of the covariance matrix for reduced computation,

$$S_{h,common}(t) = \frac{\sum_{i=1}^n \sum_{l=1}^m K_h(t_l - t) (\mathbf{y}_{il} - \bar{y}_l)(\mathbf{y}_{il} - \bar{y}_l)^T}{\sum_{i=1}^n \sum_{l=1}^m K_h(t_l - t)} = \frac{\sum_{l=1}^m K_h(t_l - t) S_l}{\sum_{l=1}^m K_h(t_l - t)}, \tag{5}$$

where S_l is the sample covariance matrix at t_l .

2.2 Sparsity and estimation in high dimensions

For high-dimensional data, the number of variables p is comparable to or even much larger than the sample size n . The estimator $\hat{U}(t)$ in Section 2.1 becomes inconsistent in this setting without additional structures. The sparsity assumption is necessary to enhance the interpretability and improve the estimates in high dimensions. Assume that $U(t) \in \mathcal{U}(q, R_q; \mathcal{T})$, where

$$\mathcal{U}(q, R_q; \mathcal{T}) = \{U(t) \in \mathbb{R}^{p \times d}, t \in \mathcal{T} | U(t) \in \mathbb{V}_{p,d}, \sup_{t \in \mathcal{T}} \max_{1 \leq j \leq d} \|\mathbf{u}_j(t)\|_q^q \leq R_q\},$$

with $0 < q \leq 1$. When $q = 0$,

$$\mathcal{U}(0, R_0; \mathcal{T}) = \{U(t) \in \mathbb{R}^{p \times d}, t \in \mathcal{T} | U(t) \in \mathbb{V}_{p,d}, \sup_{t \in \mathcal{T}} \max_{1 \leq j \leq d} \|\mathbf{u}_j(t)\|_0 \leq R_0\}.$$

The set $\mathcal{U}(q, R_q; \mathcal{T})$ is non-empty and the ℓ_q constraint is active only when $1 \leq R_q \leq p^{1-q/2}$. The family of leading eigenvectors over \mathcal{T} defined in $\mathcal{U}(q, R_q; \mathcal{T})$ generalizes the notion of static eigenvectors in [Vu and Lei \(2012\)](#). We stress that if the sparsity condition does not hold uniformly over \mathcal{T} , our method can still apply to the subregions of \mathcal{T} where this condition holds.

Recall that $\Pi(t) = U(t)U(t)^\top$ is the projection matrix. By definition, $\Pi_{jj}(t) = 0$ holds if and only if when each element of the j -th row/column of $\Pi(t)$ is zero. It implies that if $\Pi_{jj}(t) = 0$, then the corresponding j -th variable is irrelevant to the principal subspace of interest at t . Denote the support set $J(t) = \{j : \Pi_{jj}(t) > 0\}$. Apparently, the principal subspace at t does not depend on the variables outside of the set $J(t)$. For notational convenience, we introduce the following block representation of $\Sigma(t)$:

$$\begin{pmatrix} \Sigma_{JJ}(t) & \Sigma_{JJ^c}(t) \\ \Sigma_{J^c J}(t) & \Sigma_{J^c J^c}(t) \end{pmatrix}.$$

Similar block representations can be defined for other matrices and vectors.

Note that $U(t) \in \mathbb{V}_{p,d}$ where $\mathbb{V}_{p,d} = \{U \in \mathbb{R}^{p \times d} | U^\top U = I_d\}$ is the Stiefel manifold. Most existing algorithms for static sparse PCA involve a deflation step ([Shen and Huang, 2008](#); [Mackey, 2009](#)) or convex relaxation ([d'Aspremont et al., 2005](#); [Vu et al., 2013](#)) to circumvent the orthogonality constraint. In this work, motivated by (4) and taking into account the lasso-type penalty, we formulate a regularized kernel optimization problem on the Stiefel manifold,

$$\begin{aligned} \min_{U(t)} \quad & -\text{Tr}[U(t)^\top S_h(t)U(t)] + \rho_t \|U(t)\|_1 \\ \text{s.t.} \quad & U(t)^\top U(t) = I_d, \end{aligned} \tag{6}$$

where $\rho_t > 0$ is the regularization parameter at t . We allow the parameter ρ to depend on t , which makes our proposal fully adaptive to different sparsity levels varying with t . The optimization problem (6) deals with sparsity and orthogonality jointly, which can be solved effectively with a recent development called the proximal gradient method for manifold optimization ([Chen et al., 2020](#)), described in the Appendix. For more algorithmic details, we refer to [Chen et al. \(2020\)](#) and [Xiao et al. \(2018\)](#).

To improve estimation, we treat the solution of (6) as an initial estimate which is denoted by $\hat{U}^0(t)$, and then propose a refined estimate. Basically, we add a thresholding step to further filter out the variables irrelevant to the principal subspace. Denote the set of remaining variables by $\hat{J}(t) = \{j : \hat{\Pi}_{jj}^0(t) \geq \gamma_t\}$, where $\hat{\Pi}^0(t) = \hat{U}^0(t)\hat{U}^0(t)^\top$ and $\gamma_t \geq 0$ is the thresholding parameter at t . Since the estimate after thresholding may not belong to the Stiefel manifold $\mathbb{V}_{p,d}$, we re-estimate the principal eigenvectors afterwards. Our refined estimate is

$$\hat{U}(t) = \begin{pmatrix} \hat{U}_{\hat{J}(t)}(t) \\ 0 \end{pmatrix},$$

where $\hat{U}_{\hat{J}(t)}(t)$ is the solution of the problem,

$$\begin{aligned} \min_{U(t)} \quad & -\text{Tr}\{U(t)^\top S_{h,\hat{J}(t),\hat{J}(t)}(t)U(t)\} + \rho_t \|U(t)\|_1 \\ \text{s.t.} \quad & U(t)^\top U(t) = I_d. \end{aligned} \tag{7}$$

The estimated principal subspaces are given by $\hat{\mathcal{S}}(t)$ with projection matrices $\hat{\Pi}(t) = \hat{U}(t)\hat{U}(t)^\top$. The two-step estimation procedure successfully identifies the significant variables and provides consistent estimators under general l_q ($0 \leq q \leq 1$) sparsity, which is theoretically and empirically demonstrated in [Sections 3](#) and [4](#).

2.3 Tuning parameters

In this section, we discuss how to select parameters which are involved in the estimation procedure. The number of principal components d is usually fixed in advance or selected based on the fraction of explained variance (FVE). We mainly consider tuning three other parameters, the bandwidth h , the sparsity parameter ρ_t and the thresholding parameter γ_t . We suggest to select them in a sequential manner ([Chen and Lei, 2015](#); [Chen and Leng, 2016](#)). For the bandwidth h , we use the leave-one-curve-out cross-validation approach ([Rice and Silverman, 1991](#); [?](#)). Specifically, we tune the bandwidth h given $\rho_t = 0$ and $\gamma_t = 0$ by the following procedure,

$$h^* = \arg \min_{h \in \mathcal{A}_1} \frac{1}{n\bar{m}} \sum_{i=1}^n \sum_{l=1}^{m_i} \|y_{il} - \hat{U}_{h,0,0}^{-i}(t_{il})\hat{U}_{h,0,0}^{-i}(t_{il})^\top y_{il}\|^2,$$

where \mathcal{A}_1 is a candidate set of h , $\hat{U}_{h,0,0}^{-i}$ is estimated by leaving out the i -th subject with the bandwidth h , $\rho_t = 0$, $\gamma_t = 0$. Next, the parameter ρ_t is determined by k -fold cross-validation. The data is divided into k -folds by subjects, denoted by $\mathcal{D}_1, \dots, \mathcal{D}_k$. Let $\hat{U}_{h,\rho_t,\gamma_t}^{-\nu}(t)$ be the estimator

using data other than \mathcal{D}_ν at time t with parameters h , ρ_t and γ_t . Let $S_h^\nu(t)$ be the smoothed covariance matrix estimate at t with the bandwidth h . Next, we choose ρ_t given the selected bandwidth h^* and $\gamma_t = 0$ by maximizing the cross-validated inner product,

$$\rho_t^* = \arg \max_{\rho_t \in \mathcal{A}_{2,t}} \frac{1}{k} \sum_{\nu=1}^k \text{Tr}[\{\hat{U}_{h^*, \rho_t, 0}^{-\nu}(t)\}^T S_h^\nu(t) \hat{U}_{h^*, \rho_t, 0}^{-\nu}(t)],$$

where $\mathcal{A}_{2,t}$ is a candidate set for ρ_t . At last, we tune the thresholding parameter γ_t , given the selected bandwidth h^* and sparsity level ρ_t^* , by a trade-off between the explained variance $Ip(\gamma_t)$ and model complexity, i.e., the number of retained variables, where

$$Ip(\gamma_t) = \frac{1}{k} \sum_{\nu=1}^k \text{Tr}[\{\hat{U}_{h^*, \rho_t^*, \gamma_t}^{-\nu}(t)\}^T S_{h^*}^\nu(t) \hat{U}_{h^*, \rho_t^*, \gamma_t}^{-\nu}(t)],$$

where $\gamma_t \in \mathcal{A}_{3,t}$, $\mathcal{A}_{3,t}$ is a candidate set and $Ip(\gamma_t)$ is the cross-validated inner product when the threshold equals γ_t . The model complexity depicts the magnitude of the support set $\{j : \hat{\Pi}_{jj} > 0\}$. One can select the γ_t to achieve model parsimony without much information loss. We demonstrate the performance of selected parameters in [Section 4](#).

3. THEORETICAL RESULTS

In this section, we investigate theoretical properties of the proposed estimator under both common and irregular designs. To measure the performance of the estimator, we use the notion of the distance defined in [Vu and Lei \(2013\)](#). The distance between two subspaces \mathcal{E} and \mathcal{F} is

$$d^2(\mathcal{E}, \mathcal{F}) = \frac{1}{2} \|E - F\|_F^2,$$

where E and F are corresponding projection matrices.

Some assumptions necessary for theoretical results are provided, concerning the kernel functions and the properties of variables. [Assumption 1](#) is mild and routinely made in the kernel smoothing literature ([Fan and Gijbels, 1996](#); [Chen and Leng, 2016](#)).

Assumption 1. *The kernel function $K(\cdot)$ is a symmetric probability density function on $[-1, 1]$ with $\int u^2 K(u) du < \infty$ and $\int K^2(u) du < \infty$. Moreover, it is Lipschitz continuous, $|K(u) - K(v)| \leq L|u - v|$ for some positive constant L .*

This implies $K(\cdot) \leq M_K$ for a positive constant M_K . In multivariate cases, the standard assumption for sparse PCA is that x_j^2 is sub-Exponential, while [Assumption 2](#) is adapted to random processes, which holds rather generally, e.g., sub-Gaussian processes.

Assumption 2. For each $j = 1, \dots, p$, $X_j^2(t)$ is sub-Exponential uniformly in t , that is, there exists a positive constant λ_0 such that $\sup_t E e^{\lambda X_j^2(t)} < \infty$ for $|\lambda| < \lambda_0$. Also assume ε^2 is sub-Exponential.

Assumption 3. The mean $\mu_j(\cdot)$ is twice differentiable and the second derivative is bounded on \mathcal{T} for $j = 1, \dots, p$.

Assumption 4. The covariance $\sigma_{jk}(t)$ is twice differentiable and the second derivative is bounded on \mathcal{T} for $j, k = 1, \dots, p$.

The smoothness of mean and diagonal covariance functions is imposed. It is noteworthy that the $\mathbf{X}(t)$ is not necessarily smooth. First, we quantify the performance of the thresholding step by investigating the false positive control and false negative control of J . It is revealed in [Lemma 1](#) that, with a suitable parameter $\gamma(t)$, we can recover the support set consistently by the thresholding step. The condition $\min_{j \in J(t)} \Pi_{jj}(t) \geq 2\gamma(t)$ assures that the important variables can be distinguished from the noise stochastically.

Lemma 1 (Support recovery under the ℓ_q sparsity). *Recall that $\hat{\Pi}^0(t)$ is the initial estimator. Note that we have $\|\Pi(t) - \hat{\Pi}^0(t)\|_F^2 \leq C\|S_h(t) - \Sigma(t)\|_\infty = o_p(1)$ for any $t \in \mathcal{T}$. If $\min_{j \in J(t)} \Pi_{jj}(t) \geq 2\gamma(t)$ and $\gamma(t) > \|\Pi(t) - \hat{\Pi}^0(t)\|_F$, then the variable selection procedure $\hat{J}(t) := \{j : \hat{\Pi}_{jj}^0(t) \geq \gamma(t)\}$ succeeds.*

In the following, we state consistency results of the eventually obtained estimators $\hat{\mathcal{S}}(t)$. One theoretical challenge is how to carefully control the l_q ($0 \leq q \leq 1$) norm of our estimators obtained with a lasso-type penalty, which can be tackled by the consistent variable selection. Moreover, we investigate the behavior of the estimator at interior and boundary points, respectively. Note that the boundary points comprise left-boundary points $t = ch$ with $c > 0$ and right-boundary points $t = 1 - ch$ ([Fan and Gijbels, 1992](#)). Under [Assumption 1](#), they are real boundary points if $0 < c < 1$.

3.1 Rate of convergence under the irregular design

In this section, we provide theoretical results of the estimators under the irregular design. The assumption of the sampling scheme under the irregular design is provided in [Assumption 5](#).

Assumption 5. Under the irregular design, $t_{il}, i = 1, \dots, n, l = 1, \dots, m_i$ are independent and identically distributed from a density $f(\cdot)$ with compact support \mathcal{T} . In addition, the sampling density

$f_{\mathcal{T}}$ is bounded away from zero and infinity and is twice continuously differentiable with a bounded derivative on its support.

Theorem 2 (Irregular design: interior points). *Suppose that $U(t) \in \mathcal{U}(q, R_q)$. Under Assumptions 1 to 5, if $\rho(t) = M_1(t) [\{\log p/(n\bar{m}h) + \log p/n\}^{1/2} + h^2]$ and $\min_{j \in J(t)} \Pi_{jj}(t) \geq 2\gamma(t)$ where $0 < \gamma^2(t) = M_2(t) [\{\log p/(n\bar{m}h) + \log p/n\}^{1/2} + h^2]$ for any interior point t , then we have*

$$d\{\mathcal{S}(t), \hat{\mathcal{S}}(t)\} = O_p \left[\left\{ \left(\frac{\log p}{n\bar{m}h} + \frac{\log p}{n} \right)^{1/2} + h^2 \right\}^{1-q/2} \right],$$

where $\sup_t M_1(t) < \infty$ and $\sup_t M_2(t) < \infty$.

The rate of convergence at interior points incorporates two parts, the bias term h^2 and the variance term $\{\log p/(n\bar{m}h) + \log p/n\}^{1/2}$ for $q = 0$, which is consistent with that of the mean estimation in [Zhang and Wang \(2016\)](#) up to the $\log p$ term accounting for high dimensionality. Note that it differs from the conventional nonparametric scheme in that the effective sample size is $(n\bar{m}h) \wedge n$ instead of nh . Moreover, the rate is faster than that of the corresponding covariance estimation which coincides with results in the static case ([Chen and Leng, 2016](#); [Vu and Lei, 2012](#); [Cai and Zhou, 2012](#)). The bandwidth should be determined carefully to balance the bias and variance. Moreover, the sampling frequency \bar{m} plays a crucial role in the rate of convergence, which is illustrated in [Corollary 3](#).

Corollary 3. *Suppose that the conditions in Theorem 2 hold. Consider any interior point t .*

(1) *When $\bar{m}/(n/\log p)^{1/4} \rightarrow 0$ and $h = O[\{\log p/(n\bar{m})\}^{1/5}]$,*

$$d\{\mathcal{S}(t), \hat{\mathcal{S}}(t)\} = O_p \left[\left\{ \left(\frac{\log p}{n\bar{m}h} \right)^{1/2} + h^2 \right\}^{1-q/2} \right].$$

(2) *When $\bar{m}/(n/\log p)^{1/4} \rightarrow C$, where $C > 0$, and $h = O\{(\log p/n)^{1/4}\}$,*

$$d\{\mathcal{S}(t), \hat{\mathcal{S}}(t)\} = O_p \left\{ \left(\frac{\log p}{n} \right)^{1/2-q/4} \right\}.$$

(3) *When $\bar{m}/(n/\log p)^{1/4} \rightarrow \infty$, $h = o\{(\log p/n)^{1/4}\}$ and $\bar{m}h \rightarrow \infty$,*

$$d\{\mathcal{S}(t), \hat{\mathcal{S}}(t)\} = O_p \left\{ \left(\frac{\log p}{n} \right)^{1/2-q/4} \right\}.$$

When \bar{m} is relatively small as in case (1), the nonparametric rate is determined jointly by quantities n and \bar{m} . With \bar{m} grows such that $\bar{m} \gg (n/\log p)^{1/4}$, the rate achieves $(\log p/n)^{1/2-q/4}$ regardless of \bar{m} which coincides with the optimal rate for estimating static eigenvectors. Although the rates are of the same order in cases (2) and (3) which fall into the parametric paradigm, the bias in case (2) is non-vanishing (Zhang and Wang, 2016). With the advantage of data pooling, the grids are allowed to be sparse under the irregular design as long as the sample size n is moderately large. Next we provide consistency at boundary points.

Theorem 4 (Irregular design: boundary points). *Suppose that $U(t) \in \mathcal{U}(q, R_q)$. Under Assumptions 1 to 5, if $\rho(t) = M_1(t) [\{\log p/(n\bar{m}h) + \log p/n\}^{1/2} + h]$ and $\min_{j \in J(t)} \Pi_{jj}(t) \geq 2\gamma(t)$ where $0 < \gamma^2(t) = M_2(t) [\{\log p/(n\bar{m}h) + \log p/n\}^{1/2} + h]$ for any boundary point t , then we have*

$$d\{\mathcal{S}(t), \hat{\mathcal{S}}(t)\} = O_p \left[\left\{ \left(\frac{\log p}{n\bar{m}h} + \frac{\log p}{n} \right)^{1/2} + h \right\}^{1-q/2} \right],$$

where $\sup_t M_1(t) < \infty$ and $\sup_t M_2(t) < \infty$.

The variance term $\{\log p/(n\bar{m}h) + \log p/n\}^{1/2-q/4}$ is the same as that of interior points while the bias term $h^{1-q/2}$ is larger, as shown in Theorem 4. It demonstrates that the estimators at boundary points are less favorable. The phenomenon is known as boundary effect, which is typical for local constant estimators. On the practical side, boundary correction methods, e.g., boundary kernel (Gasser et al., 1985), may be applied to improve the performance at boundary points, which is out of the scope of this paper.

Corollary 5. *Suppose that the conditions in Theorem 4 hold. Consider any boundary point t .*

(1) *When $\bar{m}/(n/\log p)^{1/2} \rightarrow 0$ and $h = O[\{\log p/(n\bar{m})\}^{1/3}]$,*

$$d\{\mathcal{S}(t), \hat{\mathcal{S}}(t)\} = O_p \left[\left\{ \left(\frac{\log p}{n\bar{m}h} \right)^{1/2} + h \right\}^{1-q/2} \right].$$

(2) *When $\bar{m}/(n/\log p)^{1/2} \rightarrow C$, where $C > 0$, and $h = O\{(\log p/n)^{1/2}\}$,*

$$d\{\mathcal{S}(t), \hat{\mathcal{S}}(t)\} = O_p \left\{ \left(\frac{\log p}{n} \right)^{1/2-q/4} \right\}.$$

(3) *When $\bar{m}/(n/\log p)^{1/2} \rightarrow \infty$, $h = o\{(\log p/n)^{1/2}\}$ and $\bar{m}h \rightarrow \infty$,*

$$d\{\mathcal{S}(t), \hat{\mathcal{S}}(t)\} = O_p \left\{ \left(\frac{\log p}{n} \right)^{1/2-q/4} \right\}.$$

Similar to the results at interior points, the rate of convergence exhibits the phase transition phenomenon which occurs when $\bar{m} = O\{(n/\log p)^{1/2}\}$. To obtain the parametric rate at boundary points, the sampling frequency \bar{m} is required to be much larger than that at interior points.

3.2 Rate of convergence under the common design

In this section, we focus on the common design where sampling locations $t_l, l = 1, \dots, m$ are deterministic.

Assumption 6. *Under the common design, t_l 's are fixed and distinct, and $\max_{0 \leq l \leq m} |t_{l+1} - t_l| \leq Cm^{-1}$, where $t_0 = 0, t_{m+1} = 1$.*

Assumption 7. *The sampling frequency $m \rightarrow \infty$ and $1/(mh) = O(1)$, $h \rightarrow 0$ as $n \rightarrow \infty$.*

The Assumption 7 guarantees that $h \geq \min_{j=1, \dots, m} |t - t_j| = O(1/m)$ for each $t \in \mathcal{T}$ to avoid the trivial estimator. The rate at interior points is provided in Theorem 6.

Theorem 6 (Common design: interior points). *Suppose that $U(t) \in \mathcal{U}(q, R_q)$. Under Assumptions 1 to 4, 6 and 7, if $\rho = M_1(t) [\{\log p/(nmh) + \log p/n\}^{1/2} + h^2 + 1/m]$ and $\min_{j \in J(t)} \Pi_{jj}(t) \geq 2\gamma(t)$ where $0 < \gamma^2(t) = M_2(t) [\{\log p/(nmh) + \log p/n\}^{1/2} + h^2 + 1/m]$ for any interior point t , then we have*

$$d\{\mathcal{S}(t), \hat{\mathcal{S}}(t)\} = O_p \left[\left\{ \left(\frac{\log p}{nmh} + \frac{\log p}{n} \right)^{1/2} + h^2 + \frac{1}{m} \right\}^{1-q/2} \right],$$

where $\sup_t M_1(t) < \infty$ and $\sup_t M_2(t) < \infty$.

In contrast to the rate under the irregular design, there has an extra term $1/m$ quantifying the discretization error induced by the distinct sampling locations to approximate the integral $\int_{-1}^1 uK(u)du = 0$. Thus, the rate differs from that of mean estimation for univariate functional data under the common design in Cai and Yuan (2011). The sampling frequency is required to be large enough to obtain consistent estimates.

Corollary 7. *Suppose that $U(t) \in \mathcal{U}(q, R_q)$ and conditions in Theorem 6 hold. Consider any interior point t .*

(1) *When $m/(n/\log p)^{1/4} \rightarrow 0$ and $h = O(1/m)$,*

$$d\{\mathcal{S}(t), \hat{\mathcal{S}}(t)\} = O_p \left\{ \left(\frac{1}{m} \right)^{1-q/2} \right\}.$$

(2) When $m/(n/\log p)^{1/4} \rightarrow C$, where $C > 0$, and $h = O\{(\log p/n)^{1/4}\} = O(1/m)$,

$$d\{\mathcal{S}(t), \hat{\mathcal{S}}(t)\} = O_p \left\{ \left(\frac{1}{m} \right)^{1-q/2} \right\}.$$

(3) When $m/(n/\log p)^{1/4} \rightarrow \infty$, $h = o\{(\log p/n)^{1/4}\}$ and $mh \rightarrow \infty$, if $m/(n/\log p)^{1/2} \rightarrow 0$,

$$d\{\mathcal{S}(t), \hat{\mathcal{S}}(t)\} = O_p \left\{ \left(\frac{1}{m} \right)^{1-q/2} \right\},$$

if $m/(n/\log p)^{1/2} \rightarrow \infty$,

$$d\{\mathcal{S}(t), \hat{\mathcal{S}}(t)\} = O_p \left\{ \left(\frac{\log p}{n} \right)^{1/2-q/4} \right\}.$$

The phase transition phenomenon is more complex under the common design because of the interaction among the quantities h , n and m . The bandwidth is usually chosen to be of the order $\{\log p/(n\bar{m})\}^{1/5}$ to balance the associated bias and variance. Yet, restricted by the condition $1/(mh) = O(1)$ that guarantees observations available in the local window, the bandwidth is at least of the order $1/m$, see [Corollary 7](#). When m is relatively small, the sampling frequency m plays a dominant role in the convergence rate, i.e., $(1/m)^{1-q/2}$, which is slower than that under the irregular design. Although the rate $(1/m)^{1-q/2}$ is obtained in three cases, the difference lies in the order of optimal h . When m grows such that $m \gg (n/\log p)^{1/2}$, the parametric rate $(\log p/n)^{1/2-q/4}$ is obtained.

Theorem 8 (Common design: boundary points). *Suppose that $U \in \mathcal{U}(q, R_q)$. Under [Assumptions 1 to 4, 6 and 7](#), if $\rho = M_1(t) [\{\log p/(nmh) + \log p/n\}^{1/2} + h + 1/m]$ and $\min_{j \in J(t)} \Pi_{jj}(t) \geq 2\gamma(t)$ where $0 < \gamma^2(t) = M_2(t) [\{\log p/(nmh) + \log p/n\}^{1/2} + h + 1/m]$ for any boundary point t , then we have*

$$d\{\mathcal{S}(t), \hat{\mathcal{S}}(t)\} = O_p \left[\left\{ \left(\frac{\log p}{nmh} + \frac{\log p}{n} \right)^{1/2} + h + \frac{1}{m} \right\}^{1-q/2} \right],$$

where $\sup_t M_1(t) < \infty$ and $\sup_t M_2(t) < \infty$.

Corollary 9. *Suppose that $U(t) \in \mathcal{U}(q, R_q)$ and conditions in [Theorem 8](#) hold. Consider any boundary point t .*

(1) When $m/(n/\log p)^{1/2} \rightarrow 0$ and $h = O(1/m)$,

$$d\{\mathcal{S}(t), \hat{\mathcal{S}}(t)\} = O_p \left\{ \left(\frac{1}{m} \right)^{1-q/2} \right\}.$$

(2) When $m/(n/\log p)^{1/2} \rightarrow C$, where $C > 0$, and $h = O((\log p/n)^{1/2}) = O(\frac{1}{m})$,

$$d\{\mathcal{S}(t), \hat{\mathcal{S}}(t)\} = O_p \left\{ \left(\frac{1}{m} \right)^{1-q/2} \right\}.$$

(3) When $m/(n/\log p)^{1/2} \rightarrow \infty$, $h = o((\log p/n)^{1/2})$ and $mh \rightarrow \infty$,

$$d\{\mathcal{S}(t), \hat{\mathcal{S}}(t)\} = O_p \left\{ \left(\frac{\log p}{n} \right)^{1/2-q/4} \right\}.$$

The boundary effect also exists under the common design. By determining the optimal h , nonparametric or parametric rate is obtained depending on the sampling frequency in [Corollary 9](#). The phase transition occurs at the order of $(n/\log p)^{1/2}$ which is the same as that at interior points.

It is interesting to notice that when $m \gg (n/\log p)^{1/2}$, estimators at either boundary or interior points under the two designs achieve the optimal parametric rate. Under the irregular design, the estimator is consistent as long as $(\log p/n\bar{m}h) \vee (\log p/n) \rightarrow 0$. Thus, as the sample size permits, we can handle the extremely sparse case, that is, the sampling frequency is allowed to be very small. However, the quantity should be sufficiently large to achieve reasonable estimates under the common design. Further, when the sampling frequency is small, the irregular design is preferable to the common design with faster convergence rates.

4. SIMULATION

In this section, several experiments are conducted to evaluate the numerical performance of our proposal under independent and common designs. The observations are generated from the following model,

$$\mathbf{y}_i(t_{il}) = \sum_{k=1}^{10} \xi_{ik}(t_{il}) \mathbf{u}_k(t_{il}) + \boldsymbol{\epsilon}_{il}, \quad i = 1, \dots, n, l = 1, \dots, m_i,$$

where $\xi_{ik} \in \mathbb{R}$, $\mathbf{y}_i(t_{il}) \in \mathbb{R}^p$ and $\boldsymbol{\epsilon}_{il} \stackrel{iid}{\sim} N_p(0, \sigma^2 I_p)$. Moreover, we set $\xi_{ik}(t_{il}) \equiv \xi_{ik} \stackrel{iid}{\sim} N(0, \lambda_k)$ where $\boldsymbol{\lambda} = (30, 25, 20, 5, 3, 2, 1, 0.5, 0.2, 0.1)^T$, which follows the classical generation mechanism of functional data. The corresponding eigenvectors are sparse with only a small fraction of non-zero elements. We generate non-zero elements of $\mathbf{u}_k(t)$ as follows. First let $v_{k,(k-1)\times 5+r}(t) = \phi_r(t)$, $k = 1, \dots, 10, r = 1, \dots, 5$, where $v_{k,j}$ is the j -th element of the vector \mathbf{v}_k , $\phi_r(t)$ are functions in the Fourier basis, $\phi_r(t) = \sqrt{2} \sin(\pi(r+1)t)$ when r is odd, $\phi_r(t) = \sqrt{2} \cos(\pi r t)$ when r is even. Then $\mathbf{u}_k(t)$ are obtained by applying Gram-Schmidt or orthonormalization on $\mathbf{v}_k(t)$. Note that the locations of non-zero elements are different for different eigenvectors .

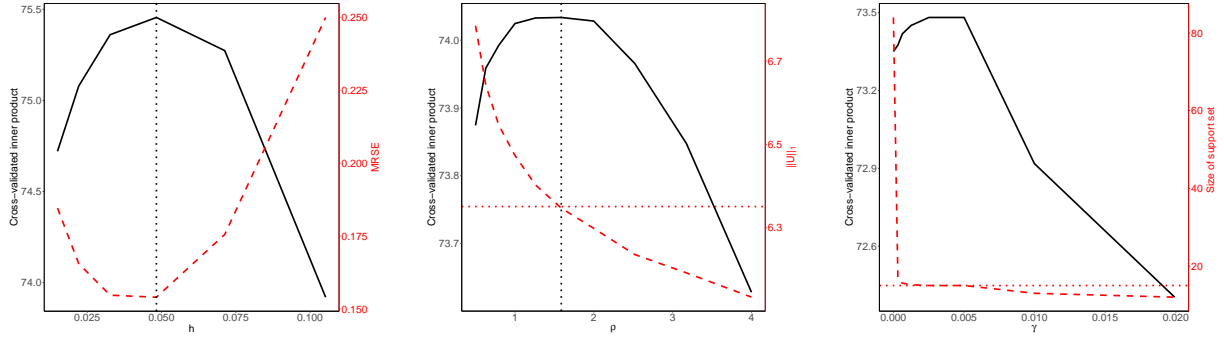


Figure 1: Common design with $p = 100, m = 100$. Left: Performance of leave-one-out cross-validation to choose bandwidth h . The right y label indicates the $MRSE(h) = m^{-1} \sum_{l=1}^m \|S_h(t_l) - \Sigma(t_l)\|_F^2$ (red dashed line). An ideal h should well approximate the $h_{ora} = \arg \min MRSE(h)$. Middle: Performance of 5-fold cross-validation to choose ρ . The right y label represents $\|U\|_1$, and an ideal ρ is where the $\|\cdot\|_1$ of estimated U (red dashed line, right y label) meets that of the true matrix (indicated by the red horizontal line). Right: The trade-off between the cross-validated inner product and the model complexity for γ given selected h and ρ . The right y label represents the size of the support set. The red dashed line shows the number of retained variables by our method varying with γ , and the red horizontal line indicates the true number of relevant variables.

Various experiments are implemented to demonstrate the effect of sample size n , sampling frequency as well as the design. For comprehensiveness, in addition to the effect of different \bar{m} with the same sample size, we also tend to illustrate how the sample size affects the estimation when the total number of observations are comparable. Thus, under the irregular design, we consider six settings for varying combinations of m_i and n . **Setting 1:** $n = 100$ and m_i are i.i.d from a discrete uniform distribution on the set $\{50, 55, 60\}$, $\bar{m} = 55$. **Setting 2:** $n = 100$ and m_i are i.i.d from a discrete uniform distribution on the set $\{20, 25, 30\}$, $\bar{m} = 25$. **Setting 3:** $n = 100$ and $m_i = m = 10$, $\bar{m} = 10$. **Setting 4:** $n = 500$ and m_i are i.i.d from a discrete uniform distribution on the set $\{10, 11, 12\}$, $\bar{m} = 11$. **Setting 5:** $n = 500$ and m_i are i.i.d from a discrete uniform distribution on the set $\{4, 5, 6\}$, $\bar{m} = 5$. **Setting 6:** $n = 500$ and $m_i = m = 2$, $\bar{m} = 2$. The time points t_{il} are i.i.d sampled from the uniform distribution on $[0,1]$. Under the common design, the data are sampled at $t_{il} = (2l)/(2m+1)$ with the sample size $n = 100$ and the sampling frequency $m = 10, 25, 55, 100$. In each setting, we generate 100 simulation runs for $p = 50, 100, 200$,

Table 1: Average integrated squared error and standard deviations over 100 replications for different settings under the irregular design.

Model		MISE ₀	MISE	MISE _{DCM}	MISE _{DCM+}
$p=100$ $n=100$	$\bar{m} = 55$	0.023 (0.010)	0.021(0.009)	0.026(0.007)	0.023(0.009)
	$\bar{m} = 25$	0.032(0.017)	0.029(0.017)	0.038(0.008)	0.047(0.025)
	$\bar{m} = 10$	0.054(0.009)	0.046(0.011)	0.186(0.222)	0.091(0.067)
$p=100$ $n=500$	$\bar{m} = 11$	0.020 (0.012)	0.019(0.012)	0.018(0.009)	0.023(0.015)
	$\bar{m} = 5$	0.028(0.017)	0.027(0.018)	0.033(0.013)	0.038(0.020)
	$\bar{m} = 2$	0.062(0.023)	0.051(0.023)	0.162(0.263)	0.074(0.025)
$p=200$ $n=100$	$\bar{m} = 55$	0.026 (0.018)	0.025(0.017)	0.048(0.021)	0.035(0.022)
	$\bar{m} = 25$	0.040(0.021)	0.038(0.021)	0.511(0.489)	0.052(0.026)
	$\bar{m} = 10$	0.069(0.026)	0.066(0.026)	0.948(0.451)	0.099(0.062)
$p=200$ $n=500$	$\bar{m} = 11$	0.022 (0.013)	0.020(0.013)	0.046(0.045)	0.030(0.019)
	$\bar{m} = 5$	0.033(0.020)	0.032(0.020)	0.373(0.421)	0.044(0.021)
	$\bar{m} = 2$	0.066(0.025)	0.065(0.025)	0.876(0.421)	0.083(0.026)

respectively.

Table 2: Average integrated squared error and standard deviations over 100 replications for different settings under the common design.

Model		MISE ₀	MISE	MISE _{DCM}	MISE _{DCM+}
$p=100$ $n=100$	$m=100$	0.016 (0.005)	0.014(0.004)	0.021(0.009)	0.014(0.007)
	$m=55$	0.025(0.005)	0.023(0.003)	0.027(0.009)	0.024(0.006)
	$m=25$	0.043(0.005)	0.042(0.005)	0.059(0.052)	0.044(0.007)
	$m=10$	0.203(0.049)	0.202(0.049)	0.228(0.157)	0.209(0.054)
$p=200$ $n=100$	$m=100$	0.016(0.005)	0.015(0.004)	0.031(0.012)	0.024(0.008)
	$m=55$	0.026(0.006)	0.024(0.006)	0.065(0.069)	0.043(0.009)
	$m=25$	0.052(0.011)	0.051(0.011)	0.560(0.553)	0.252(0.218)
	$m=10$	0.227(0.058)	0.212(0.044)	1.559(0.252)	1.306(0.077)

We set $d = 3$, and other parameters are chosen as discussed in [Section 2.3](#). Specifically, the bandwidth h and the sparsity level ρ are selected by leave-one-curve-out and 5-fold cross-validation, respectively, while the thresholding parameter γ is determined by a trade off between the explained variance and the model complexity, i.e., the number of retained variables. The selected parameters well depict the true smoothness of covariance matrices, the sparsity level and model complexity of the eigenvectors, respectively, see [Figure 1](#) for a detailed illustration. For comprehensive comparison, we also estimate eigenvectors by performing PCA on matrices obtained by dynamic covariance models (DCM) ([Chen and Leng, 2016](#)). Since the tuning parameters are selected by leave-one-point-out in DCM which is inappropriate for repeated measurements, we use leave-one-curve-out instead and denote the resulting model by DCM+. To reduce the computation, we tune the parameters depending on t at a few reference points and use the selected parameter of the reference point which is closest to the target evaluation point. We evaluate the performance of estimators by the mean integrated squared error $\sum_{i=1}^{100} \int d_i^2(U(t), \hat{U}(t)) dt / 100$ and denote the error of our initial, refined, the DCM and DCM+ estimators by $\text{MISE}_0, \text{MISE}, \text{MISE}_{DCM}$ and MISE_{DCM+} , respectively. Moreover, the results of boundary (i.e., $[0, h]$ or $[1-h, 1]$) and interior points (i.e., $[h, 1-h]$) using the average integrated squared error scaled by the length of interval are provided in the Appendix.

The results for $p=100$ and 200 are summarized in [Tables 1](#) and [2](#), while the results for $p = 50$ are qualitatively similar and are not reported for space economy. Our refined estimators perform somewhat better than the initial estimates under both designs. Under the irregular design, as noted in [Section 3.1](#), the grids can be sparse to obtain reasonable estimation as the sample size permits. Thus, even in the very sparse case as $\bar{m} = 2$ or 5 , the error is still well controlled and even smaller than that when $\bar{m} = 10$ due to larger sample size and the advantage of data pooling. Moreover, when the total observations are comparable, larger sample size usually leads to better estimates. Under the common design, it is shown in [Table 2](#) and [Figure 2](#) (top, left), the estimates improve as m increases, and the improvement is more obvious for small m . For the same sample size and relatively small sampling frequency, the irregular design tends to obtain better estimates. For moderately large m , i.e., $m = 55$, the estimators achieve comparable performance for the two designs, see [Tables 1](#) and [2](#), which implies that the estimation may yield parametric rate.

It is observed from [Tables 1](#) and [2](#) that the estimators obtained using dynamic covariance

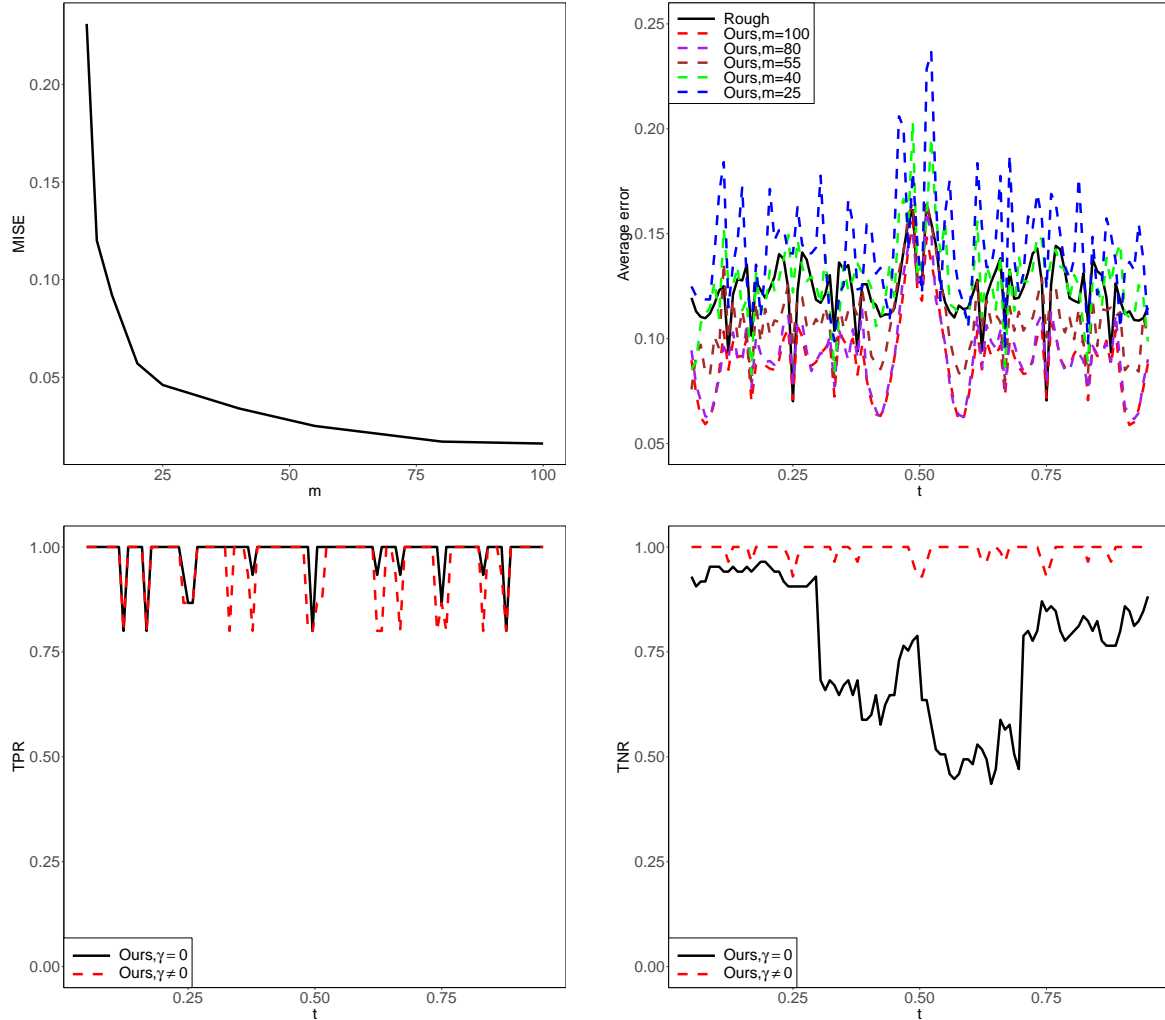


Figure 2: The common design: $n = 100, p = 100$. Top left: Effect of different sampling frequencies m on the performance of the proposed estimates. Top right: Comparison of performances between rough (solid line) and the proposed estimates (dashed lines) under different m over 100 evaluated time points over $[0.05, 0.95]$. The bottom panel: Comparison of TPR (left) and TNR (right) over t between the proposed estimates with $\gamma_t = 0$ (black, solid) or not (red, dashed). Our refined estimators with thresholding have advantage in screening out irrelevant variables and thus achieving desired model parsimony.

matrices perform worse than the proposal, especially when p is large and the observational grids are sparse. Even though the model DCM+ improves the estimates, it is still inferior to our approach. Such empirical findings demonstrate the superiority of our method in estimating dynamic principal subspaces for high-dimensional data with repeated measurements. For space savings, the results of

boundary and interior points are deferred to the Appendix. In contrast to the interior estimators, the boundary estimates lead to larger error under both designs.

Furthermore, to demonstrate the advantage of smoothing, we compare results between our approach and the rough estimators obtained by replacing S_h with sample covariance matrices in (6) under the common design over 100 evaluation times. As illustrated in Figure 2 (top, right), the proposed estimators achieve better performance when m approximately exceeds 55, which reveals that our estimation can benefit from increasing the number of observations while the rough estimators can not. To illustrate the performance of the refined estimates in achieving model parsimony, two criteria $TNR = TN/(TN+FP)$ and $TPR=TP/(TP+FN)$ are reported in Figure 2, where TP and TN are abbreviations for true positives and true negatives, respectively, i.e., the number of significant or non-significant variables correctly identified by our method, similarly FP and FN stand for false positives and false negatives. The bottom panel in Figure 2 reveals the fact that the refined estimate by thresholding yields better variable selection results, which is particularly useful for model interpretation.

5. REAL DATA

We apply the proposed method to analyze the features of the data from HCP 900 subjects release. The data consists of $n = 330$ subjects who are healthy young adults, in which each subject is asked to walk for 2 minutes and the distance in feet is recorded. Also, each subject participates in a motor task, where participants are asked to act according to presented visual cues, such as tapping their fingers, moving their tongue. During the task, the brain of each subject is scanned and the neural activities are recorded at 284 equispaced time points. After preprocessing, the average BOLD (blood-oxygen-level dependent) signals at 68 different brain regions are obtained. The details of experiment and data acquisition can be found in the reference manual of WU-Minn HCP 900 Subjects Data Release that is available on the website of human connectome project.

We focus on modeling the dynamic principal subspaces spanned by the first $d = 5$ leading eigenvectors. The corresponding eigenvalues satisfy the eigen-gap assumption, which have multiplicity 1 in the whole course. Other regularity parameters are chosen as discussed in Section 2.3. In the analysis, we normalize the 284 scanning time points onto $[0, 1]$. The heatmaps of 10×10 sub-matrices of estimated projection matrices using our method and the rough method at four

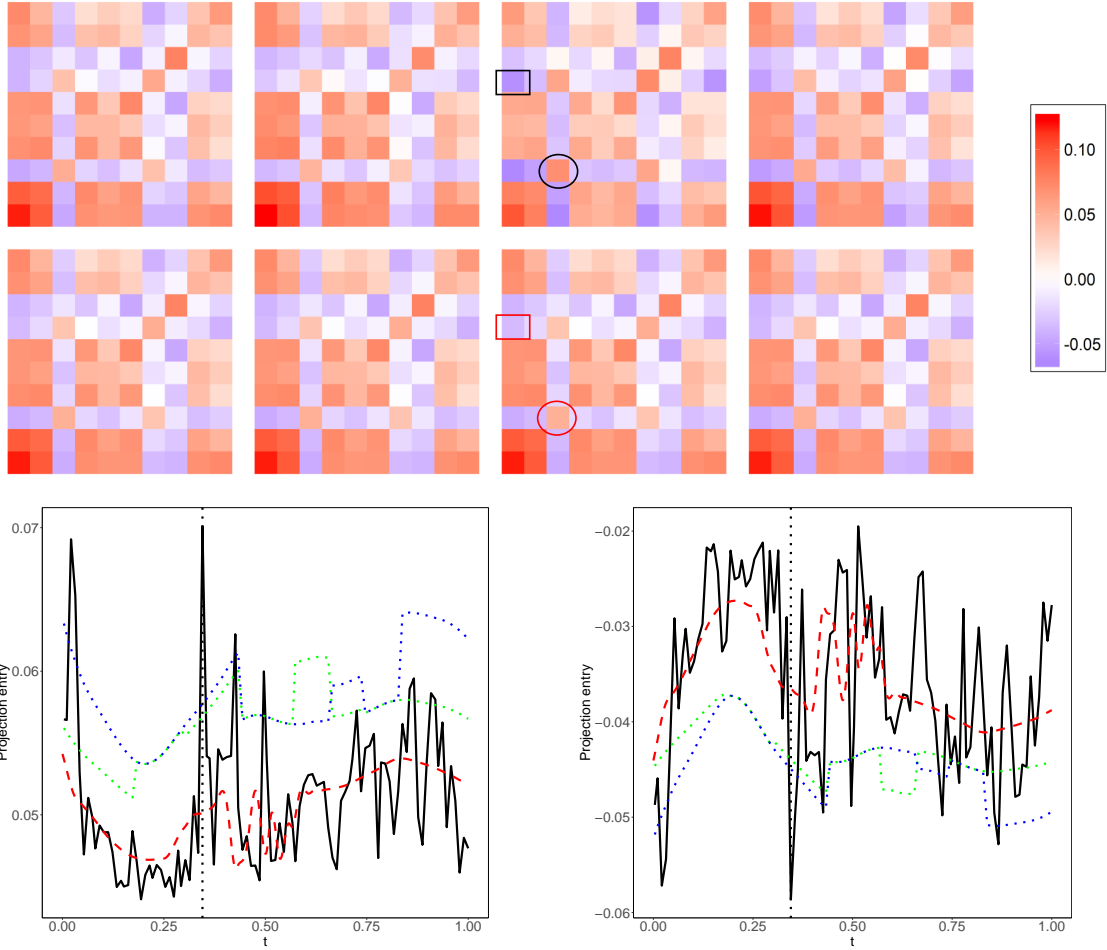


Figure 3: The top panel: Heatmaps of 10×10 sub-matrix of the estimated projection matrix at four adjacent evaluated time points for better visualization. The first row: the rough estimator, the second row: the proposed estimator. The bottom panel: Selected entries from the sub-matrix of the projection matrix varying with t for the HCP data. The left: the selected entry indicated by the circle. The right: the selected entry indicated by the square. Black, solid: the rough estimator; Green, dotted: DCM; Blue, dotted: DCM+; Red, dashed: the proposed estimator. The vertical dotted line indicates the time point where the the heatmaps in the third column are plotted.

evaluated time points 92/284, 95/284, 98/284 and 101/284 are shown in the top panel of [Figure 3](#). As we can see, the estimators obtained using sample covariance matrices fluctuate wildly at 98/284, while our estimates vary rather smoothly. For better visualization, we pick two entries from the sub-matrix, marked by the square and circle, respectively, and plot the time-varying trend of them in the bottom panel of [Figure 3](#). Furthermore, the estimates of DCM and DCM+ are provided in [Figure 3](#) for comparison. The result reveals that our method is favorable to obtain smooth and reasonable estimates.

6. DISCUSSIONS

We propose a unified framework to estimate dynamic principal subspaces in high-dimensional settings by combining the local smoothing and sparsity constraint. Our estimators satisfy sparsity and orthogonality simultaneously. Different from the conventional nonparametric smoothing, the rates of convergence depend on the sampling frequency and sample size jointly. When the sampling frequency is suitably large, the obtained rates are optimal as if the whole curves are available under both designs. Otherwise, the nonparametric rate should be considered and the irregular design is preferred with faster rate of convergence.

It is well-known that the principal eigenvector is identifiable (up to the sign change) if the eigengap condition holds. If this condition is satisfied over the entire \mathcal{T} , then the dynamic principal eigenvector is smooth ([Berrendero et al., 2011](#)). Otherwise, we allow the principal eigenvectors to be nonsmooth or discontinuous. In contrast, [Shao and Yao \(2020\)](#) aimed to estimate a smooth function $e_k(t)$ while allowing discontinuous eigenvalues $\lambda_k(t)$ in low-dimensional settings by applying smoothing splines on manifolds, which essentially differs from our goal in this work. The $e_k(t)$ defined in their paper is not necessarily the eigenvector corresponding to the k -th largest eigenvalue at t due to the order changing of eigenvalues. If all involved eigenvectors in $e_k(t)$ are estimable by our method, we can manually change the sign and order by minimizing the distance at two successive points to obtain smooth $e_k(t)$. However, it is complex and unclear how to well estimate a smooth $e_k(t)$ in high-dimensional settings since it may involve eigenvectors corresponding to the smallest few eigenvalues at some t , which is leaved for future study.

References

Absil, P.-A., Mahony, R. and Sepulchre, R. (2009) *Optimization algorithms on matrix manifolds*. Princeton University Press.

Berrendero, J. R., Justel, A. and Svarc, M. (2011) Principal components for multivariate functional data. *Computational Statistics & Data Analysis*, **55**, 2619–2634.

Bickel, P. J. and Levina, E. (2008) Covariance regularization by thresholding. *The Annals of Statistics*, **36**, 2577–2604.

Cai, T. T. and Yuan, M. (2011) Optimal estimation of the mean function based on discretely sampled functional data: Phase transition. *The Annals of Statistics*, **39**, 2330–2355.

Cai, T. T. and Zhou, H. H. (2012) Minimax estimation of large covariance matrices under ℓ_1 -norm. *Statistica Sinica*, 1319–1349.

Chen, K. and Lei, J. (2015) Localized functional principal component analysis. *Journal of the American Statistical Association*, **110**, 1266–1275.

Chen, S., Ma, S., Man-Cho So, A. and Zhang, T. (2020) Proximal gradient method for nonsmooth optimization over the stiefel manifold. *SIAM Journal on Optimization*, **30**, 210–239.

Chen, Z. and Leng, C. (2016) Dynamic covariance models. *Journal of the American Statistical Association*, **111**, 1196–1207.

d'Aspremont, A., Ghaoui, L. E., Jordan, M. I. and Lanckriet, G. R. (2005) A direct formulation for sparse pca using semidefinite programming. In *Advances in Neural Information Processing Systems*, 41–48.

Edelman, A., Arias, T. A. and Smith, S. T. (1998) The geometry of algorithms with orthogonality constraints. *SIAM Journal on Matrix Analysis and Applications*, **20**, 303–353.

Fan, J. and Gijbels, I. (1992) Variable bandwidth and local linear regression smoothers. *The Annals of Statistics*, 2008–2036.

— (1996) Local polynomial modelling and its applications. *Monographs on Statistics and Applied Probability*. Chapman & Hall/CRC.

Gasser, T., Müller, H.-G. and Mammitzsch, V. (1985) Kernels for nonparametric curve estimation. *Journal of the Royal Statistical Society. Series B (Methodological)*, 238–252.

Johnstone, I. M. and Lu, A. Y. (2009) On consistency and sparsity for principal components analysis in high dimensions. *Journal of the American Statistical Association*, **104**, 682–693.

Li, Y. and Hsing, T. (2010) Uniform convergence rates for nonparametric regression and principal component analysis in functional/longitudinal data. *The Annals of Statistics*, **38**, 3321–3351.

Ma, Z. (2013) Sparse principal component analysis and iterative thresholding. *The Annals of Statistics*, **41**, 772–801.

Mackey, L. W. (2009) Deflation methods for sparse pca. In *Advances in Neural Information Processing Systems*, 1017–1024.

Ramsay, J. O. and Silverman, B. W. (2005) *Functional data analysis*. Springer, New York, 2nd edition.

Rice, J. A. and Silverman, B. W. (1991) Estimating the mean and covariance structure nonparametrically when the data are curves. *Journal of the Royal Statistical Society. Series B (Methodological)*, 233–243.

Shen, H. and Huang, J. Z. (2008) Sparse principal component analysis via regularized low rank matrix approximation. *Journal of Multivariate Analysis*, **99**, 1015–1034.

Vu, V. and Lei, J. (2012) Minimax rates of estimation for sparse pca in high dimensions. In *Artificial intelligence and statistics*, 1278–1286.

Vu, V. Q., Cho, J., Lei, J. and Rohe, K. (2013) Fantope projection and selection: A near-optimal convex relaxation of sparse pca. In *Advances in Neural Information Processing Systems*, 2670–2678.

Vu, V. Q. and Lei, J. (2013) Minimax sparse principal subspace estimation in high dimensions. *The Annals of Statistics*, **41**, 2905–2947.

Witten, D. M., Tibshirani, R. and Hastie, T. (2009) A penalized matrix decomposition, with applications to sparse principal components and canonical correlation analysis. *Biostatistics*, **10**, 515–534.

Xiao, X., Li, Y., Wen, Z. and Zhang, L. (2018) A regularized semi-smooth newton method with projection steps for composite convex programs. *Journal of Scientific Computing*, 1–26.

Yin, J., Geng, Z., Li, R. and Wang, H. (2010) Nonparametric covariance model. *Statistica Sinica*, **20**, 469–479.

Yuan, Y., Zhu, H., Lin, W. and Marron, J. (2012) Local polynomial regression for symmetric positive definite matrices. *Journal of the Royal Statistical Society: Series B (Statistical Methodology)*,

74, 697–719.

Zhang, X. and Wang, J.-L. (2016) From sparse to dense functional data and beyond. *The Annals of Statistics*, **44**, 2281–2321.

Zhu, H., Chen, Y., Ibrahim, J. G., Li, Y., Hall, C. and Lin, W. (2009) Intrinsic regression models for positive-definite matrices with applications to diffusion tensor imaging. *Journal of the American Statistical Association*, **104**, 1203–1212.

Zou, H., Hastie, T. and Tibshirani, R. (2006) Sparse principal component analysis. *Journal of Computational & Graphical Statistics*, **15**, 265–286.

A. ALGORITHM

We use the retraction-based proximal gradient method (ManPG) (Chen et al., 2020) to solve our manifold optimization problem (6). Denote $\mathcal{M} = \mathbb{V}_{p,d}$ and $F(U) = -\text{Tr}\{U(t)^T S_h(t) U(t)\} + \rho \|U(t)\|_1$ where $f(U) = -\text{Tr}\{U(t)^T S_h(t) U(t)\}$ is Lipschitz continuous with the Lipschitz constant L and $h(U) = \rho \|U(t)\|_1$. ManPG first computes a descent direction D_k (k -th step) by solving the following problem:

$$\begin{aligned} \min_D \quad & \langle \nabla f(U_k), D \rangle + \frac{1}{2t} \|D\|_F^2 + h(U_k + D) \\ \text{s.t.} \quad & D^T U_k + U_k^T D = 0, \end{aligned} \tag{A.1}$$

where U_k is obtained in the k -th iteration, $t > 0$ is a step size and D is a descent direction of F in the tangent space $T_{U_k} \mathcal{M}$. Based on the Lagrangian function and KKT system, we get that

$$E(\Lambda) = \mathcal{A}_k(D(\Lambda)) = 0, \tag{A.2}$$

where $\mathcal{A}_k(D) = D^T U_k + U_k^T D$, $D(\Lambda) = \text{prox}_{th}(B(\Lambda)) - U_k$ with $B(\Lambda) = U_k - t(\nabla f(U_k) - \mathcal{A}^*(\Lambda))$, $\mathcal{A}^*(\Lambda)$ denotes the adjoint operator of \mathcal{A}_k , where Λ is a $d \times d$ symmetric matrix. We will use semi-smooth Newton method (SSN) (Xiao et al., 2018) to solve (A.2).

Retraction operation is an important concept in manifold optimization, see Absil et al. (2009) for more details. There are many common retractions for the Stiefel manifold, including exponential mapping, the polar decomposition and the Cayley transformation. We adopt the exponential mapping (Edelman et al., 1998),

$$\text{Retr}_U(tD) = \begin{bmatrix} U & Q \end{bmatrix} \exp \left(t \begin{bmatrix} -U^T D & -R^T \\ R & 0 \end{bmatrix} \right) \begin{bmatrix} I_d \\ 0 \end{bmatrix},$$

Algorithm 1 Manifold Proximal Gradient Method (ManPG) for Solving (6).

Input: Initial point $U_0 \in \mathbb{V}_{p,d}$, $\delta \in (0, 1)$, $\gamma \in (0, 1)$, Lipschitz constant L

```
1: for  $k \in 0, 1, \dots$  do
2:   Obtain  $D_k$  by solving the subproblem (A.1) with  $t \in (0, 1/L]$ ;
3:   Set  $\alpha = 1$ 
4:   while  $F(\text{Retr}_{U_k}(\alpha D_k)) > F(U_k) - \delta \alpha \|D_k\|_F^2$  do
5:      $\alpha = \gamma \alpha$ 
6:   end while
7:   Set  $U_{k+1} = \text{Retr}_{U_k}(\alpha D_k)$ 
8: end for
```

where $QR = -(I_d - UU^T)D$ is the unique QR factorization.